Journal of
Intelligent Material
Systems and Structures

Original Article

Journal of Intelligent Material Systems and Structures
2015, Vol. 26(16) 2242–2255

DOI: 10.1177/1045389X14551434
jim.sagepub.com
SAGE

A hysteresis nonlinear model of giant magnetostrictive transducer

Yuchuan Zhu and Yuesong Li

Abstract

In order to describe the hysteresis nonlinear performance of giant magnetostrictive transducer, based on the relationship between complex permeability and magnetization, eddy current effects of Terfenol-D, and kinetic characteristic of giant magnetostrictive transducer, a new hysteresis nonlinear model is developed, which consists of quasi-static model and dynamic model considering eddy current effect of Terfenol-D, dynamic of power amplifier, and magnetic aftereffect in the magnetization process. After that, to identify model parameters and improve the accuracy of the proposed model, an experiment platform is established and a modified hysteresis nonlinear model is put forward. Finally, experiments are conducted to demonstrate the effectiveness of the modified model and the corresponding identification method. The modified model prediction results of giant magnetostrictive transducer agree well with experiment results not only under quasi-static operating conditions but also under dynamic operating conditions. Additionally, the proposed model's parameters have definite physical meaning, but the parameters to be identified are less and model expression is more simple than that of the other hysteresis nonlinear models such as the Jiles–Atherton model. The present model can be used in the simulation and performance prediction of giant magnetostrictive transducer, which is especially suitable for the real-time control system of giant magnetostrictive transducer.

Keywords

Eddy current effect, magnetic hysteresis, giant magnetostrictive transducer, dynamic model, complex permeability

Introduction

Giant magnetostrictive transducer opened the way to develop totally new electromechanical devices with higher energy density, faster response, and better precision than previously possible, such as sound and vibration (Wakiwaka et al., 1997), sonar system (Jenner et al., 2000), active vibration control (Braghin et al., 2012; Hiller et al., 1989), magnetostrictive motors (Kiesewetter, 1988), hydraulics (Karunanidhi and Singaperumal, 2010; Li et al., 2011a; Yoo and Wereley, 2004), and sensors (Yamamoto et al., 1997). However, like other smart material actuators (e.g. piezoelectric actuator and shape memory alloy actuator), giant magnetostrictive transducers display strong hysteresis, which makes their effective use quite challenging, and hysteresis nonlinearity makes them difficult to control giant magnetostrictive transducer, which has serious influence on the positioning precision of giant magnetostrictive transducer.

Hysteresis nonlinear model plays an important role to predict and optimize the performance of giant magnetostrictive transducer, and at present, the hysteresis nonlinear modeling for giant magnetostrictive transducer can roughly be classified into two kinds: physics-based models and phenomenological models. An example of physics-based models is the Jiles–Atherton model of ferromagnetic hysteresis (Jiles and Atherton, 1986), which is built on first principles of physics. Phenomenological models only reflect the characteristics between input and output, which is a black box model based on experimental data; a popular phenomenological hysteresis model adopted for giant magnetostrictive transducer is the Preisach model (Adly et al., 1991; Cruz-Hernandez and Hayward, 2001; Gorbet et al., 1998; Hughes and Wen, 1994). Smith (1997) employed a Preisach model to describe saturation and hysteresis nonlinearities observed in a magnetostrictive actuator mounted on a cantilever

College of Mechanical and Electrical Engineering, Nanjing University of Aeronautics and Astronautics, Nanjing, China

Corresponding author:
Yuchuan Zhu, College of Mechanical and Electrical Engineering, Nanjing University of Aeronautics and Astronautics, 29 Yudao St., Nanjing 210016, China.
Email: meeyczhu@nuaa.edu.cn

beam. Because the classical Preisach operator is rate independent, which is different from the actual hysteresis nonlinearity in giant magnetostrictive transducer, "dynamic" generalizations of the Preisach operator were proposed by assuming output-rate-dependent Preisach density functions (Mayergoyz, 1991) or input-rate-dependent behavior of delayed relays (Bertotti, 1992). Then, the frequency-dependent hysteresis (Tan and Baras, 2004) is conveniently described using the Preisach integral method. Similar to the Preisach model, another popular phenomenological hysteresis model is the Prandtl–Ishlinskii model; unlike the discontinuous relay operators in the Preisach model, the Prandtl–Ishlinskii (Al Janaideh, 2009) model is constructed using continuous play or stop hysteresis operators which are characterized by the input and the threshold. The Prandtl–Ishlinskii model has been proposed as an operator-based model to characterize the hysteresis properties of giant magnetostrictive transducer, which offers greater flexibility and unique property so that its inverse can be attained analytically. However, the Prandtl–Ishlinskii model can neither exhibit asymmetric hysteresis loops nor saturated hysteresis output; in response to this issue, a rate-dependent Prandtl–Ishlinskii model (Aljanaideh et al., 2014) integrating a memoryless function of deadband operator was subsequently formulated to describe both the rate dependence and the asymmetric hysteresis loops of the magnetostrictive actuator in addition to the output saturation.

Physics-based models, such as the Jiles–Atherton model (Jiles and Atherton, 1984, 1986), have the advantage of relying on intuitive development, which helps with design and facilitates extension of the model to new types of actuators, and then, the Jiles–Atherton model is extended to include the effects of stress (Dapino et al., 2000; Sablik and Jiles, 1993). Furthermore, the Jiles–Atherton model is developed to quantify the strains and output displacements by the giant magnetostrictive transducers (Dapino et al., 2000a,b). Another physics-based model is the Stoner–Wohlfarth model; the original Stoner–Wohlfarth model is modified for magnetostrictive materials (Jiles and Thoelke, 1994; Park et al., 2002). In this model, the rotation of noninteracting magnetic domains is the main mechanism, and magnetostriction is introduced by adding an energy term to the domain energy, but the model is not useful in some applications, such as controller design, where accuracy is very important.

However, physics-based models usually include many complicated physical parameters that are difficult to be identified (Almeida et al., 2001; Calkins et al., 2000; Cao et al., 2004), such as saturation magnetization intensity, saturation magnetostriction, averaged energy of the pinning sites, and. Phenomenological models, such as Preisach model, provide an empirical estimation of the relationship between input and output of experimental data, which need more experimental data and involve complicated calculation.

Besides aiming to describe the complex nonlinear constitutive behavior of Terfenol-D measured in the experiments, numerous nonlinear models have been established, including the dynamic hysteresis constitutive model (Zheng et al., 2009), energy-averaged model (Chakrabarti and Dapino, 2012), dynamic loss hysteresis model (Xu et al., 2013), nonlinear transient constitutive model (Wang and Zhou, 2010), and so on. However, among these models, it is a purely material constitutive model and does not incorporate the structural dynamic behavior arising from the transducer operation; nonetheless, magnetostriction is the phenomenon of strong coupling between magnetic state and mechanical state of magnetostrictive materials. A general hysteresis nonlinear model considering material constitutive model and the structural dynamic behavior is extremely significant from a practical point of view.

Additionally, generally speaking, a good hysteresis nonlinear model should have the following properties: agree well with experiments, computationally simple and efficient, and reasonably easy to determine transducer parameters. In this article, we mainly focus on the complex hysteresis behavior of the giant magnetostrictive actuator system under magnetically biased conditions and mechanically biased conditions. Based on the relationship between complex permeability and magnetization intensity, a new hysteresis nonlinear model is developed, which consists of quasi-static hysteresis nonlinear model and dynamic hysteresis nonlinear model considering eddy current effect and dynamic of power amplifier. In order to improve the accuracy of the model, additionally, a modified hysteresis nonlinear model is presented as well. The present model's parameters have definite physical meaning just like the Jiles–Atherton model, but the parameters to be identified are lesser than those of the Jiles–Atherton model and model expression is more simple than that of Preisach model, which is more suitable for the real-time control system of giant magnetostrictive transducer. The present model can be used in the simulation and performance prediction of giant magnetostrictive transducer.

Configuration of giant magnetostrictive transducer

Figure 1 illustrates the configuration of giant magnetostrictive transducer, mainly consisting of permanent magnet, giant magnetostrictive material (GMM) rod (Terfenol-D rod is used in this research), output rod, coil, and spring. The spring applies a prestress on GMM rod because a larger magnetostrictive strain can be obtained with same magnetic field when GMM rod is compressed (Evans and Dapino, 2010). Permanent

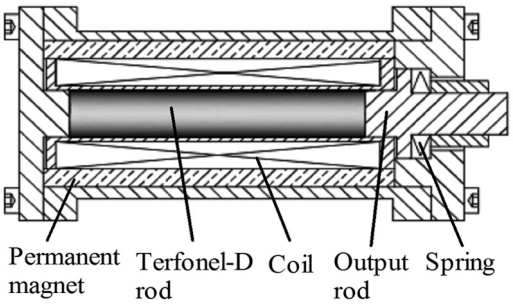

Figure 1. Configuration of giant magnetostrictive transducer.

magnet is used for providing a longitudinal magnetic bias, which can improve the sensitivity of GMM rod and eliminate frequency doubling. When the sign of magnetic field produced by the coil is the same as the sign of magnetic bias, the length of GMM rod elongates. If the sign of magnetic field produced by the coil and the sign of magnetic bias are opposite, the length of GMM rod is shorter than that in the initial condition.

Quasi-static hysteresis nonlinear model

At quasi-static condition, the energy conversion process in giant magnetostrictive transducer involves three stages: the stage from the electrical energy to the magnetic energy, the stage from the magnetic energy to the elastic potential energy, and the stage from the elastic potential energy to the mechanical energy. So, the model of giant magnetostrictive transducer involves three submodels from the viewpoint of energy conversion. The first submodel is the magnetization model which describes the relationship between applied exciting current and magnetization of GMM rod. The second submodel is the magnetoelastic model describing the relationship between magnetostrictive strain and magnetization. The third submodel is output displacement model of giant magnetostrictive transducer describing the relationship between the output displacement and magnetostrictive strain of giant magnetostrictive transducer.

Magnetization model of GMM rod

In a closed magnetic circuit, the applied magnetic field H generated by an alternating current i is given by

$$H = \frac{Ni}{k_{\mathrm{f}} L_{\mathrm{G}}} = \frac{NI_{\mathrm{m}}}{k_{\mathrm{f}} L_{\mathrm{G}}} \cos \omega t = H_{\mathrm{m}} \cos \omega t \tag{1}$$

where N is the number of excitation coil turns, I_{m} is the amplitude of the alternating current, k_{f} is the leakage coefficient of the magnetic flux, L_{G} is the length of GMM rod, H_{m} is the amplitude of applied magnetic field, and ω is the angular frequency.

The complex number form of the applied magnetic field is written as (Engdahl, 1999)

$$\tilde{H} = H_{\mathrm{m}} e^{j\omega t} \tag{2}$$

In a sinusoidal magnetic field, the relative permeability of GMM rod is a complex number, and the complex number form of magnetic flux density is given by

$$\tilde{B} = \mu_0(\mu' - j\mu'')\tilde{H} = \mu_0 H_{\mathrm{m}} \left[\mu' e^{j\omega t} + \mu'' e^{j(\omega t - \pi/2)}\right] \tag{3}$$

So, the magnetic flux density B in GMM rod can be written as

$$\begin{aligned} B &= \mu_0 \mu' H_{\mathrm{m}} \cos \omega t + \mu_0 \mu'' H_{\mathrm{m}} \cos\left(\omega t - \frac{\pi}{2}\right) \\ &= \mu_0 H(\mu' + \mu'' \tan \omega t) \end{aligned} \tag{4}$$

where μ_0 is the permeability of free space, μ' is the real part of the complex relative permeability, and μ'' is the imaginary part of the complex relative permeability.

The magnetization M can be deduced from magnetic flux density B and the applied magnetic field H

$$M = \frac{B}{\mu_0} - H = H(\mu' - 1 + \mu'' \tan \omega t) \tag{5}$$

Consider relative permeability $\mu_{\mathrm{r}} = \mu' - j\mu''$, so

$$\mu' = \sqrt{|\mu_{\mathrm{r}}|^2 - (\mu'')^2} \tag{6}$$

Substituting equations (1) and (6) into equation (5) yields

$$M = H_{\mathrm{m}} \left(\left(\sqrt{|\mu_{\mathrm{r}}|^2 - (\mu'')^2} - 1 \right) \cos \omega t + \mu'' \sin \omega t \right) \tag{7}$$

Rewriting equation (7) leads to

$$M = \sqrt{\left(\sqrt{|\mu_{\mathrm{r}}|^2 - (\mu''_{\mathrm{h}})^2} - 1 \right)^2 + (\mu''_{\mathrm{h}})^2} H_{\mathrm{m}} \cos(\omega t - \theta_{\mathrm{h}}) \tag{8}$$

where θ_{h} is the lag angle caused by hysteresis

$$\theta_{\mathrm{h}} = \arctan \left(\frac{\mu''_{\mathrm{h}}}{\sqrt{|\mu_{\mathrm{r}}|^2 - (\mu''_{\mathrm{h}})^2} - 1} \right) \tag{9}$$

Equations (8) and (9) are valid for low-frequency sinusoidal magnetic field.

Magnetoelastic model of GMM rod

As discussed in Li and Zhu (2012), the magnetostrictive λ is given by

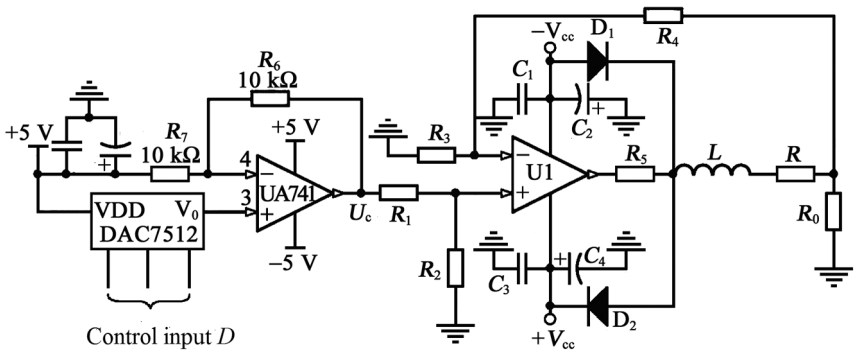

Figure 2. Circuit diagram of power amplifier.

$$\lambda = \frac{3}{2}\frac{\lambda_S}{M_S^2}M^2 \tag{10}$$

where λ_S and M_S are the saturation magnetostrictive and the saturation magnetization, respectively.

GMM rod practical magnetic field distribution consists of bias magnetic field H_b and control magnetic field H_c, and accordingly, GMM rod practical magnetization consists of bias magnetization M_b and control magnetization M_c; hence, equation (10) can be written as follows

$$\begin{aligned}\lambda &= \frac{3}{2}\frac{\lambda_S}{M_S^2}M^2(H_c + H_b) - \frac{3}{2}\frac{\lambda_S}{M_S^2}M_b^2 \\ &= k_\lambda\left[M^2(H_c + H_b) - M_b^2\right]\end{aligned} \tag{11}$$

where k_λ is the magnetostrictive coefficient, which can be obtained from saturation magnetostrictive and the saturation magnetization or from experimental data. $M(\bullet)$ is the function of magnetic field.

If an experimental point (λ_0, M_0) has been known, k_λ can be calculated from the following equation

$$k_\lambda = \frac{\lambda_0}{M^2(H_0 + H_b) - M_b^2} \tag{12}$$

Output displacement model of giant magnetostrictive transducer

Output displacement y of giant magnetostrictive transducer can be written as follows according to Hooke's law

$$\frac{Ky}{A_G} = E^H\lambda \tag{13}$$

where K is the equivalent stiffness of GMM rod.

Substituting equation (11) into equation (13) yields

$$y = \frac{E^H A_G\lambda}{K} = k_\lambda\frac{E^H A_G}{K}\left[M^2(H_c + H_b) - M_b^2\right] \tag{14}$$

If an experimental point (H_0, y_0) has been known

$$\begin{aligned}y_0 = k_\lambda\frac{E^H A_G}{K}\left(M_0^2 - M_b^2\right) = \frac{k_\lambda E^H A_G(|\mu_r| - 1)^2}{K} \\ \left[(H_0 + H_b)^2 - H_b^2\right]\end{aligned} \tag{15}$$

Substituting equation (15) into equation (14) yields

$$y = \frac{M^2(H_c + H_b) - (|\mu_r| - 1)^2H_b^2}{(|\mu_r| - 1)^2\left[(H_0 + H_b)^2 - H_b^2\right]}y_0 \tag{16}$$

Because the applied magnetic field H_c is small, the resultant magnetic field varied around the bias magnetic field H_b; based on equation (7) and the principle of linear superposition, the resultant magnetization in low excitation frequency yields

$$\begin{aligned}M(H_c + H_b) = \sqrt{\left(\sqrt{(|\mu_r| - 1)^2 - (\mu''_h)^2} - 1\right)^2 + (\mu''_h)^2} \\ H_m\cos(\omega t - \theta_h) + (|\mu_r| - 1)H_b\end{aligned} \tag{17}$$

Dynamic hysteresis nonlinear model

At dynamic condition, two dynamic processes are considered: dynamic of power amplifier and dynamic of giant magnetostrictive transducer. Dynamic of power amplifier is the dynamic process from input voltage of power supply to input current of drive coil. Dynamic of giant magnetostrictive transducer is the dynamic process from the point of view of the energy; the energy conversion process in giant magnetostrictive transducer involves three stages: the stage from the electrical energy to the magnetic energy, where eddy current effect and hysteresis effect will be included; the stage from the magnetic energy to the elastic potential energy; and the stage from the elastic potential energy to the mechanical energy. So, the model of giant magnetostrictive transducer involves three submodels. The first submodel is the dynamic magnetization model

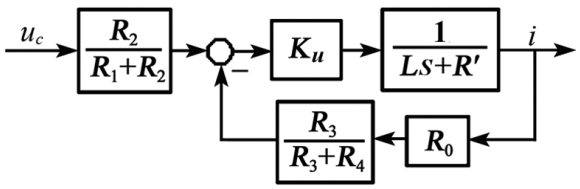

Figure 3. Transfer function block diagram of power amplifier.

which describes the relationship between applied exciting current and magnetization of GMM rod. The magnetoelastic model describing the relationship between magnetostrictive strain and magnetization is the second submodel, which is the same as the above-mentioned quasi-static hysteresis model of giant magnetostrictive transducer. The final submodel is the kinetic model of giant magnetostrictive transducer describing the relationship between the output displacement and magnetostrictive strain.

Dynamic model of power amplifier

Drive coil is an inductance element which makes input current lag behind input voltage. So, in order to obtain fast current response, we designed a power amplifier with integrated power amplifiers by depth electric current negative feedback technology, which can eliminate input current lag, and its circuit diagram and transfer function block diagram are shown in Figures 2 and 3, respectively.

The transfer function of power amplifier can be written as follows according to Figure 3

$$i = \frac{R_2}{R_1 + R_2} \frac{K_u}{Ls + R + R_5} \frac{u_c}{1 + \frac{K_u}{Ls + R + R_5} \frac{{R_3}^{R_0}}{{R_3}^{+}R_4}} \tag{18}$$

Assuming $R_1 = R_2$ and $R_3 = R_4$, equation (18) can be rewritten as follows

$$\begin{aligned} i &= \frac{K_u}{Ls + R + R_5} \frac{u_c}{2\left(1 + \frac{K_u}{Ls + R + R_5} \frac{R_0}{2}\right)} \\ &= \frac{K_u u_c}{2Ls + (2R + 2R_5 + K_u R_0)} \end{aligned} \tag{19}$$

where K_u is the open-loop gain of the integrated operational amplifier, u_c is the input voltage, L is the inductance of drive coil, and R and R_0 are resistance of the drive coil and sampling resistance, respectively.

Dynamic magnetization model of GMM rod

A time-varying magnetic field Maxwell equation can be written as follows

$$\nabla \times \mathbf{H} = \mathbf{J} + \frac{\partial \mathbf{D}}{\partial t} \tag{20}$$

$$\nabla \times \mathrm{E} = -\frac{\partial \mathbf{B}}{\partial t} \tag{21}$$

$$\nabla \cdot \mathbf{B} = 0 \tag{22}$$

$$\nabla \cdot \mathbf{D} = \rho \tag{23}$$

$$\mathbf{D} = \varepsilon \mathbf{E} \tag{24}$$

$$\mathbf{B} = \mu \mathbf{H} \tag{25}$$

$$\mathbf{J} = \gamma \mathbf{E} \tag{26}$$

Consider the rotation on both sides of equation (20)

$$\nabla \times \nabla \times \mathbf{H} = \nabla \times \mathbf{J} + \nabla \times \frac{\partial \mathbf{D}}{\partial t} \tag{27}$$

Substituting equations (21), (24), and (26) into equation (27) yields

$$\nabla \times \nabla \times \mathbf{H} = -\gamma \frac{\partial \mathbf{B}}{\partial t} - \varepsilon \frac{\partial^2 \mathbf{B}}{\partial t^2} \tag{28}$$

Assuming the change in magnetic flux density B to be independent of the change in stress on the GMM and substituting equation (25) into equation (28) yield

$$\nabla \times \nabla \times \mathbf{H} = -\gamma\mu \frac{\partial \mathbf{H}}{\partial t} - \varepsilon\mu \frac{\partial^2 \mathbf{H}}{\partial t^2} \tag{29}$$

As is well known, the vector identical relation

$$\nabla \times \nabla \times \mathbf{H} = \nabla(\nabla \cdot \mathbf{H}) - \nabla^2 \mathbf{H} \tag{30}$$

Substituting equations (22) and (25) into equation (30) yields

$$\nabla \times \nabla \times \mathbf{H} = -\nabla^2 \mathbf{H} \tag{31}$$

Substituting equation (31) into equation (29) yields

$$\nabla^2 \mathbf{H} = \gamma\mu \frac{\partial \mathbf{H}}{\partial t} + \varepsilon\mu \frac{\partial^2 \mathbf{H}}{\partial t^2} \tag{32}$$

The second term on the right-hand side of equation (32) can be neglected for the frequency range in which magnetostrictive transducers are operated ($\gamma \gg \omega\varepsilon$). So, equation (32) can be rewritten as follows

$$\nabla^2 \mathbf{H} = \gamma\mu \frac{\partial \mathbf{H}}{\partial t} \tag{33}$$

In a high-frequency sinusoidal magnetic field, we can obtain GMM rod practical magnetic field distribution in a frequency characteristic form from equation (33)

$$\nabla^2 \mathbf{H} = j\omega\gamma\mu \mathbf{H} \tag{34}$$

We can simplify GMM rod practical magnetic field distribution as one-dimensional axial direction (z direction) as shown in Figure 4.

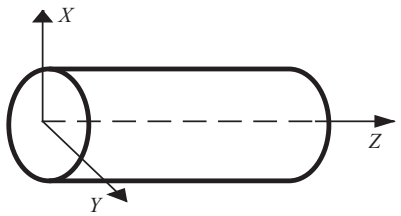

Figure 4. Cylindrical coordinate system of GMM rod.
GMM: giant magnetostrictive material.

According to the cylindrical coordinate system of GMM rod, in the z direction, equation (34) can be rewritten as follows

$$\nabla^2 H = j\omega\gamma\mu H \tag{35}$$

Equation (35) can be rearranged, and the applied magnetic field H yields (Braghin et al., 2011; Yang et al., 2008)

$$\frac{\mathrm{d}^2\dot{H}}{\mathrm{d}r^2} + \frac{1}{r}\frac{\mathrm{d}\dot{H}}{\mathrm{d}r} = j\omega\gamma\mu\dot{H} \tag{36}$$

Consider boundary conditions

$$\dot{H}(r_\mathrm{G}, t) = H_\mathrm{m} e^{j\omega t} \tag{37}$$

where r_G is the radius of GMM rod.

Thus, the solution of equation (36) is

$$\dot{H}(r, t) = \frac{J_0(r\sqrt{-j\omega\gamma\mu})}{J_0(r_\mathrm{G}\sqrt{-j\omega\gamma\mu})} H_\mathrm{m} e^{j\omega t} \tag{38}$$

where $J_0(\bullet)$ is the zero-order Bessel function.

In GMM rod axes

$$\dot{H}(0, t) = \frac{J_0(0)}{J_0(r_\mathrm{G}\sqrt{-j\omega\gamma\mu})} H_\mathrm{m} e^{j\omega t} = \frac{1}{J_0(r_\mathrm{G}\sqrt{-j\omega\gamma\mu})} H_\mathrm{m} e^{j\omega t} \tag{39}$$

By the definition of imaginary variation Bessel function (Li et al., 2011a)

$$J_0\left(r_\mathrm{G}\sqrt{-j\omega\gamma\mu}\right) = \mathrm{ber}\left(r_\mathrm{G}\sqrt{\omega\gamma\mu}\right) + j\mathrm{bei}\left(r_\mathrm{G}\sqrt{\omega\gamma\mu}\right) \tag{40}$$

where $\mathrm{ber}(\bullet)$ and $\mathrm{bei}(\bullet)$ are the real part and the imaginary part of Bessel function, respectively.

Substituting equation (40) into equation (39), GMM rod practical magnetic field distribution

$$\dot{H} = \frac{\mathrm{ber}\left(r_\mathrm{G}\sqrt{\omega\gamma\mu}\right) - j\mathrm{bei}\left(r_\mathrm{G}\sqrt{\omega\gamma\mu}\right)}{\mathrm{ber}^2\left(r_\mathrm{G}\sqrt{\omega\gamma\mu}\right) + \mathrm{bei}^2\left(r_\mathrm{G}\sqrt{\omega\gamma\mu}\right)} H_\mathrm{m} e^{j\omega t} \tag{41}$$

Rewriting equation (40) in real form yields

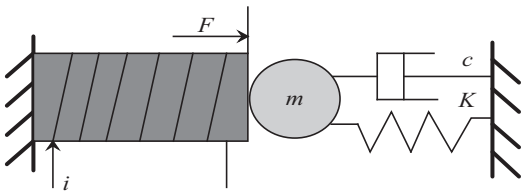

Figure 5. Lumped parameter model of giant magnetostrictive transducer.

$$H = \frac{\mathrm{ber}\left(r_\mathrm{G}\sqrt{\omega\gamma\mu}\right) H_\mathrm{m} \cos \omega t}{\mathrm{ber}^2\left(r_\mathrm{G}\sqrt{\omega\gamma\mu}\right) + \mathrm{bei}^2\left(r_\mathrm{G}\sqrt{\omega\gamma\mu}\right)} + \frac{\mathrm{ber}\left(r_\mathrm{G}\sqrt{\omega\gamma\mu}\right) H_\mathrm{m} \cos\left(\omega t - \frac{\pi}{2}\right)}{\mathrm{ber}^2\left(r_\mathrm{G}\sqrt{\omega\gamma\mu}\right) + \mathrm{bei}^2\left(r_\mathrm{G}\sqrt{\omega\gamma\mu}\right)} \tag{42}$$

Rearranging equation (42) leads to

$$H = \frac{1}{\sqrt{\mathrm{ber}^2\left(r_\mathrm{G}\sqrt{\omega\gamma\mu}\right) + \mathrm{bei}^2\left(r_\mathrm{G}\sqrt{\omega\gamma\mu}\right)}} H_\mathrm{m} \cos(\omega t - \theta_\mathrm{e}) \tag{43}$$

where θ_e is the lag angle caused by eddy

$$\theta_\mathrm{e} = \arctan\left(\frac{\mathrm{bei}\left(r_\mathrm{G}\sqrt{\omega\gamma\mu}\right)}{\mathrm{ber}\left(r_\mathrm{G}\sqrt{\omega\gamma\mu}\right)}\right) \tag{44}$$

From simultaneous equations (8), (9), (43), and (44), the dynamic magnetization model of GMM rod can be written as follows considering the eddy current effect

$$M = \sqrt{\frac{\left(\sqrt{|\mu_\mathrm{r}|^2 - (\mu''_\mathrm{h})^2} - 1\right)^2 + (\mu''_\mathrm{h})^2}{\mathrm{ber}^2\left(r_\mathrm{G}\sqrt{\omega\gamma\mu}\right) + \mathrm{bei}^2\left(r_\mathrm{G}\sqrt{\omega\gamma\mu}\right)}}\, H_\mathrm{m} \cos(\omega t - \theta_\mathrm{h} - \theta_\mathrm{e}) \tag{45}$$

Kinetic model of giant magnetostrictive transducer

The lumped parameter model of giant magnetostrictive transducer is a mass–spring–damping system (Tan and Baras, 2004), as shown in Figure 5. Therefore, the model of giant magnetostrictive transducer can be described as

$$F = m\frac{\mathrm{d}^2 y}{\mathrm{d}t^2} + c\frac{\mathrm{d}y}{\mathrm{d}t} + Ky \tag{46}$$

where y is the output displacement of giant magnetostrictive transducer; and m, c, and K are the equivalent mass, equivalent damping, and equivalent stiffness of giant magnetostrictive transducer, respectively.

The magnetostrictive force F is defined as

$$F = A_\mathrm{G} E^\mathrm{H} \lambda \tag{47}$$

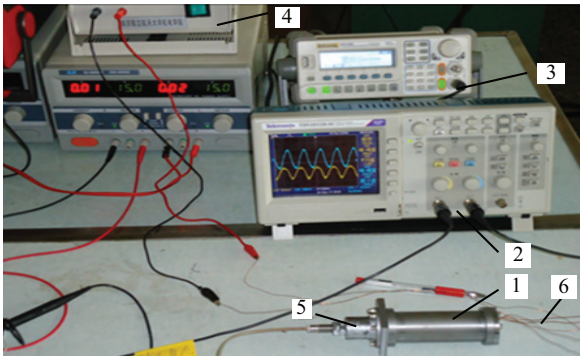

Figure 6. Photograph of the experiment platform: (1) giant magnetostrictive transducer, (2) oscilloscope, (3) signal generator, (4) power amplifier, (5) displacement sensor, and (6) sensing coil.

where A_G and E^H are the cross-sectional area and the elastic modulus of GMM rod, respectively.

Inserting equation (46) into equation (47) and using Laplace transforms yield

$$y = \frac{A_G E^H \lambda}{ms^2 + cs + K} \tag{48}$$

From simultaneous equations (11), (45), and (48), a dynamic hysteresis nonlinear displacement model of giant magnetostrictive transducer can be obtained.

Experiment platform and parameter identification

Experiment platform

The precision of the present giant magnetostrictive transducer hysteresis nonlinear model needs to be verified by experimental data; therefore, the experiment platform used for measuring the performance of giant magnetostrictive transducer is built and is shown in Figure 6, which consists of signal generator, adjustable power supply, constant current power amplifier, giant magnetostrictive transducer, eddy current sensor, and oscilloscope.

The giant magnetostrictive transducer is driven by alternating current from power amplifier which is controlled by the sinusoidal signal generated by signal generator, and the sinusoidal signal is displayed in the oscilloscope with the output signal of displacement sensor. Due to current negative feedback, the phase of the output current of the power amplifier is basically synchronous with the input voltage signal. The gain of constant current power amplifier is 2 A/V.

Parameter identification

Coil inductance L with GMM rod and coil inductance L_0 without GMM rod in giant magnetostrictive transducer meet

Table 1. Model parameters for giant magnetostrictive transducer.

Parameters	Value
Radius of GMM rod (r_G) (mm)	5
Length of GMM rod (L_G) (mm)	80
Equivalent mass of giant magnetostrictive transducer (m) (kg)	0.1
Equivalent damping of giant magnetostrictive transducer (c) (N s/m)	3000
Equivalent stiffness of giant magnetostrictive transducer (K) (N/m)	9.9×10^6
Bias magnetization (M_b) (kA/m)	250
Leakage coefficient of the magnetic flux (K_f)	1.2
Number of the excitation coil (N) (turns)	1300
Young's modulus of GMM rod (E^H) (GPa)	20
Equivalent time constant of power amplifier τ(ms)	0.2
Electric conductivity of GMM rod (γ) (S)	1.67×10^6
Inductance of drive coil (L) (mH)	6
Resistance of drive coil (R) (Ω)	6
Sampling resistance (R_0) (Ω)	0.5

$$L = |\mu_r| L_0 \tag{49}$$

We can obtain $|\mu_r| = 5$ by the measured value of L and L_0 around the bias magnetic field.

In the present model and at quasi-static operation conditions, the output displacement of giant magnetostrictive transducer meets equation (16), and only two parameters need to be identified: the magnetostrictive coefficient k_λ and the imaginary part of relative complex permeability μ_h''; the other parameters are known and are shown in Table 1.

Because the lag angle caused by hysteresis increases with the amplitude value of the applied magnetic field, the value of imaginary part of relative complex permeability has a positive correlation with the amplitude value of the input current, so we assume

$$\mu_h'' = k_u I_m \tag{50}$$

where k_u is the parameter to be identified and I_m is the amplitude value of the input current.

Assuming the amplitude value of the input current $I_0 = 0.5$ A and frequency of the input current $f = 1$ Hz, we make the minimum square sum of difference value between simulation curves with test curves, which is shown in Figure 7. Thus, we obtain the imaginary part of the relative complex permeability $\mu_h'' = 1.1$.

If an experimental point (H_0, y_0) has been known based on equation (15), the magnetostrictive coefficient k_λ can be written as follows

$$k_\lambda = \frac{y_0 K}{E^H A_G (|\mu_r| - 1)^2 \left[(H_0 + H_b)^2 - H_b^2 \right]} \tag{51}$$

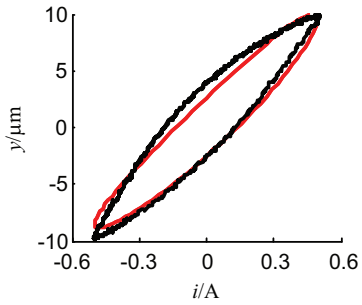

Figure 7. Identification of the imaginary part for relative complex permeability.

Therefore, we can obtain $k_\lambda = 1.4694 \times 10^{-14}$ m^2/A^2.

Hysteresis nonlinear model validation

Quasi-static hysteresis nonlinear model validation

To verify the validity and applicable scope of the above-mentioned model equations (16) and (17), we obtained quasi-static output displacement under input current amplitude I_m = 0.25, 0.5, 0.7, and 1 A by simulation and experiment, respectively, which are shown in Figure 8.

As shown in Figure 8, under quasi-static operating conditions, the model prediction results overestimate the amplitude and phase of hysteresis loop under input current amplitude of 0.25 A and, on the other hand, underestimate the amplitude and phase of hysteresis loop under input current amplitudes of 0.7 and 1 A but have a good agreement with the experimental data under input current amplitude of 0.5 A.

Dynamic hysteresis nonlinear model validation

Consider the same input current amplitude value of 0.8 A and the different input current exciting frequencies of 10, 50, 80, 100, 150, and 200 Hz. Thus, we obtained dynamic output displacement simulation curves and experiment curves as shown in Figure 9.

As shown in Figure 9, under dynamic operating conditions, the model prediction results underestimate the amplitude and phase of hysteresis loop under input current exciting frequencies of 10, 50, and 80 Hz and, on

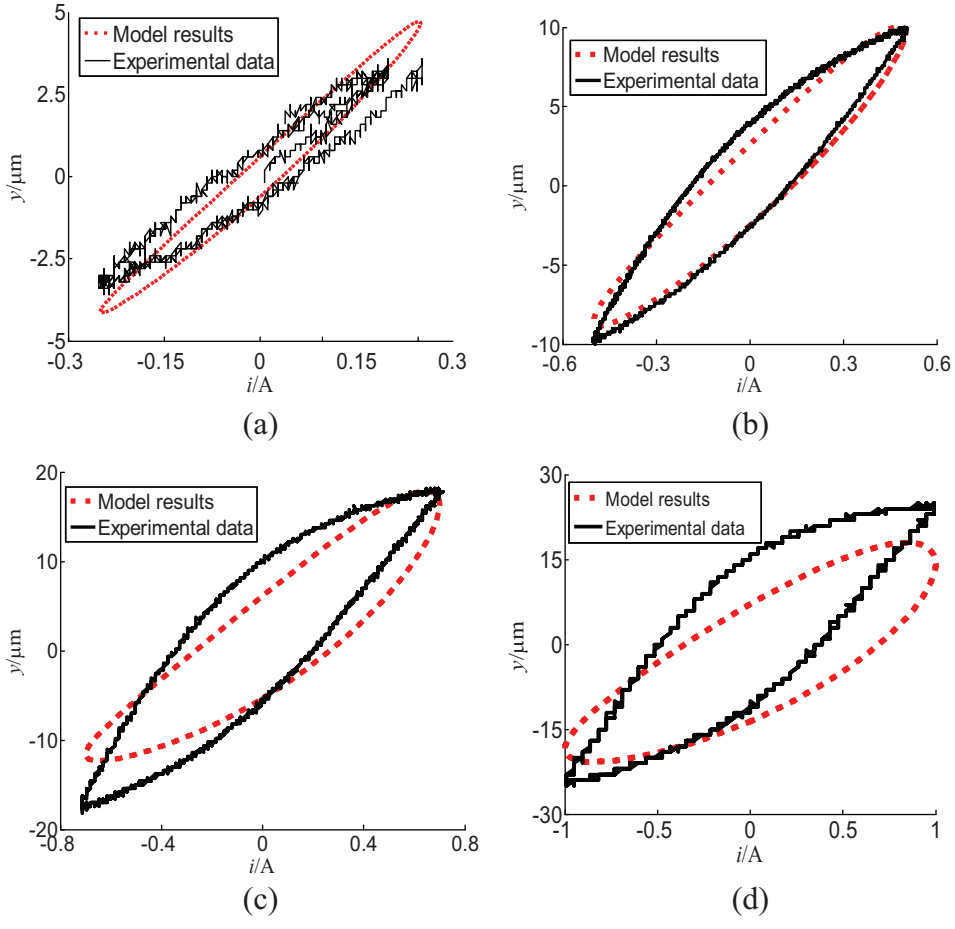

Figure 8. Verification for the quasi-static hysteresis nonlinear model of giant magnetostrictive transducer: (a) I_m = 0.25 A, (b) I_m = 0.5 A, (c) I_m = 0.7 A, and (d) I_m = 1 A.

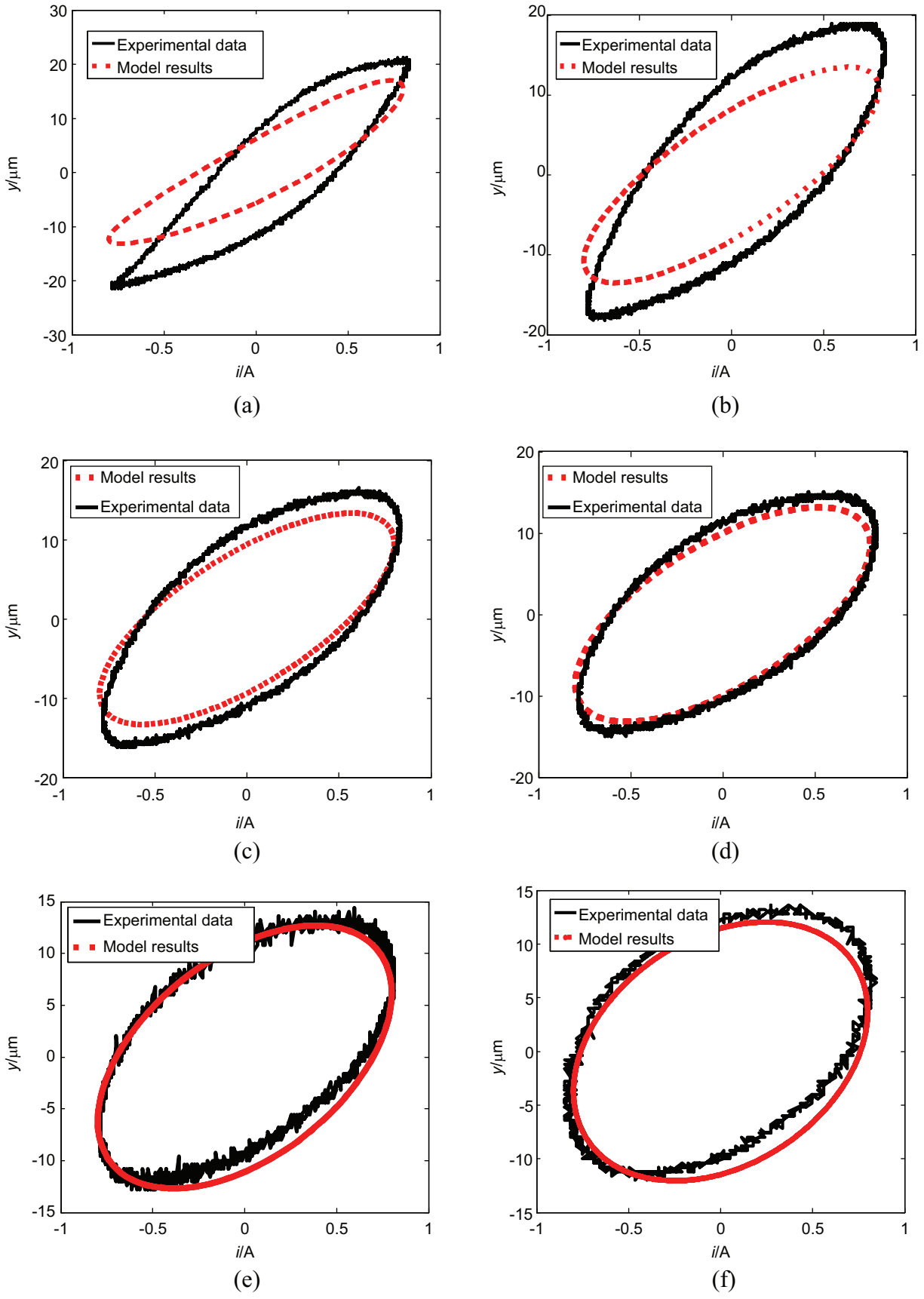

Figure 9. Verification for the dynamic hysteresis nonlinear model of giant magnetostrictive transducer: (a) 10 Hz, (b) 50 Hz, (c) 80 Hz, (d) 100 Hz, (e) 150 Hz, and (e) 200 Hz.

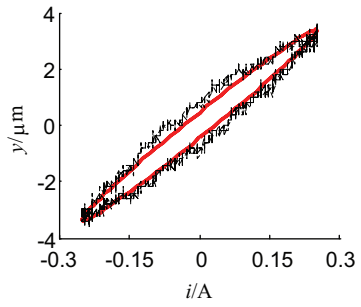

Figure 10. Identification of the correction term.

the other hand, have a good agreement with the experimental data under input current exciting frequencies of 100, 150, and 200 Hz.

Modified hysteresis nonlinear model and model validation

Modified quasi-static hysteresis nonlinear model and model validation

Figure 8 shows that simulation results have a better agreement with experiment result under input current amplitude $I_0 = 0.5$ A than that under other input current amplitudes. The reason is that the imaginary part of relative complex permeability is identified under input current amplitude $I_m = 0.5$ A. So, when input current amplitude is not equal to 0.5 A, the above-mentioned quasi-static hysteresis nonlinear model needs to be modified. We assume that the correction term of quasi-static hysteresis nonlinear model is proportional to the difference between the input current amplitude I_m and the reference input current amplitude $I_0 = 0.5$ A; thus, we can obtain the modified quasi-static hysteresis nonlinear model of giant magnetostrictive transducer as follows

$$y = \frac{M^2(H_c + H_b) - (|\mu_r| - 1)^2 H_b^2}{(H_0 + H_b)^2 - H_b^2} y_0 + \frac{(I_m - I_0)\hat{y}_0}{(|\mu_r| - 1)} \tag{52}$$

where $\hat{y}_0$ is the unknown parameter and has to be identified.

Assuming the input current amplitude value of 0.25 A and the input current frequency $f = 1$ Hz, we make the minimum square sum of difference value between simulation curves based on equation (52) with test curves, which is shown in Figure 10. Thus, we obtained the unknown parameter to be identified $\hat{y}_0 \approx 13$.

In order to verify the validity and reliability of the modified hysteresis quasi-static nonlinear model, quantitative comparisons between its predictions and experimental data are given. We obtained output displacement under input current amplitude $I_m = 0.25$, 0.5, 0.7, and 1 A by the modified model formula (52) and experimental data, respectively, which is shown in Figure 11.

Comparing with Figures 8 and 11, it is observed that the modified quasi-static hysteresis nonlinear model yields output displacement precision higher than that of unmodified one. The reason for the difference between the mentioned hysteresis nonlinear model and the modified one is the nonlinear constitutive behavior of Terfenol-D and the structural behavior of transducer mechanical system.

As shown in Figure 11, although the modified model precision decreases slightly with the amplitude value of the input current, however, when the amplitude value of the input current is within 1 A, the modified model results of giant magnetostrictive transducer have a perfect agreement with the majority experiment results.

Additionally, as shown in Figure 11, the difference between the modified hysteresis nonlinear model and experimental data is mainly symmetry of hysteresis loop of giant magnetostrictive transducer, that is, the hysteresis loop controlled by the modified hysteresis nonlinear model is symmetrical; however, on this actual transducer system, the hysteresis loop drawn by experimental data is asymmetrical for discontinuous damping reduction in the magnetization process and structure defect of GMM.

Modified dynamic hysteresis nonlinear model and model validation

Similar to the method used by modified quasi-static hysteresis nonlinear model, based on the kinetic model of giant magnetostrictive transducer, we can obtain the modified dynamic hysteresis nonlinear model of giant magnetostrictive transducer as follows

$$y(s) = \frac{M^2(H_c + H_b) - (|\mu_r| - 1)^2 H_b^2}{(|\mu_r| - 1)^2 \left[(H_0 + H_b)^2 - H_b^2\right]} y_0 + \frac{(I_m - I_0)\hat{y}_0}{ms^2 + Cs + K} K \tag{53}$$

where $M(H_c + H_b)$ is the synthesis of magnetization considering eddy effect and bias magnetization effect. Considering equations (17) and (43), $M(H_c + H_b)$ can be written as follows

$$M(H_c + H_b) = L_f H_m \cos(\omega t - \theta_h - \theta_e) + (|\mu_r| - 1)H_b \tag{54}$$

$$L_f = \sqrt{\frac{\left(\sqrt{|\mu_r|^2 - (\mu''_h)^2} - 1\right)^2 + (\mu''_h)^2}{\mathrm{ber}^2(r_G\sqrt{\omega\gamma\mu}) + \mathrm{bei}^2(r_G\sqrt{\omega\gamma\mu})}} \tag{55}$$

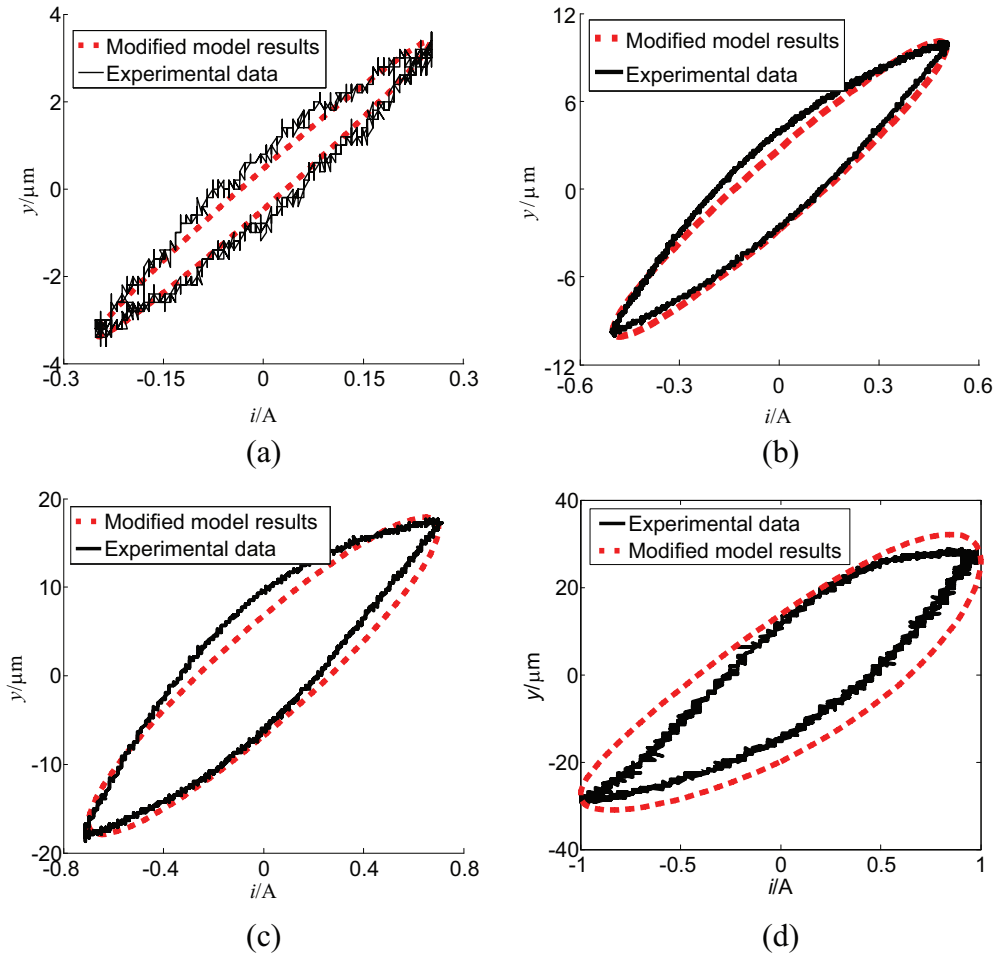

Figure 11. Verification for the quasi-static modified hysteresis nonlinear model of giant magnetostrictive transducer: (a) I_m = 0.25 A, (b) I_m = 0.5 A, (c) I_m = 0.7 A, and (d) I_m = 1 A.

where L_f represents the impact on output displacement considering eddy effect and hysteresis effect.

Equation (53) is the output displacement theoretical model of giant magnetostrictive transducer; in the actual application system, the dynamic process of giant magnetostrictive transducer also includes power amplifier dynamic, magnetic aftereffect dynamic, and so on; thus, equation (53) can be rewritten as follows

$$y(s) = \frac{M^2(H_c + H_b) - (|\mu_r| - 1)^2 H_b^2}{(|\mu_r| - 1)^2 \left[(H_0 + H_b)^2 - H_b^2\right]} \frac{y_0 + (I_m - I_0)\hat{y}_0}{ms^2 + Cs + K} \frac{K}{\tau s + 1} \quad (56)$$

where τ is the time constant of power amplifier dynamic and magnetic aftereffect dynamic for giant magnetostrictive transducer.

Consider the same input current amplitude value of 0.8 A and the different input current exciting frequencies of 10, 50, 80, 100, 150, and 200 Hz. The comparisons between the simulation results predicted by the modified dynamic hysteresis nonlinear model and experimental data under dynamic operating conditions are shown in Figure 12. As is evident in these six figures, the above modified model simulation results are perfectly coincident with the experimental data. It confirms that the modified dynamic nonlinear model established in this article can quantitatively describe the complex hysteresis behavior of the giant magnetostrictive transducer system under dynamic operating conditions within exciting frequencies of 100 Hz.

Conclusion

Based on the relationship between complex permeability and magnetization, eddy current effects of Terfenol-D, and kinetic model of giant magnetostrictive transducer, a novel general hysteresis nonlinear model is established in this article for the giant magnetostrictive transducer system, in which strong coupling interaction between the nonlinear constitutive behavior of Terfenol-D and the structural dynamic behavior of transducer system itself is modeled, which consists of quasi-static hysteresis nonlinear model and

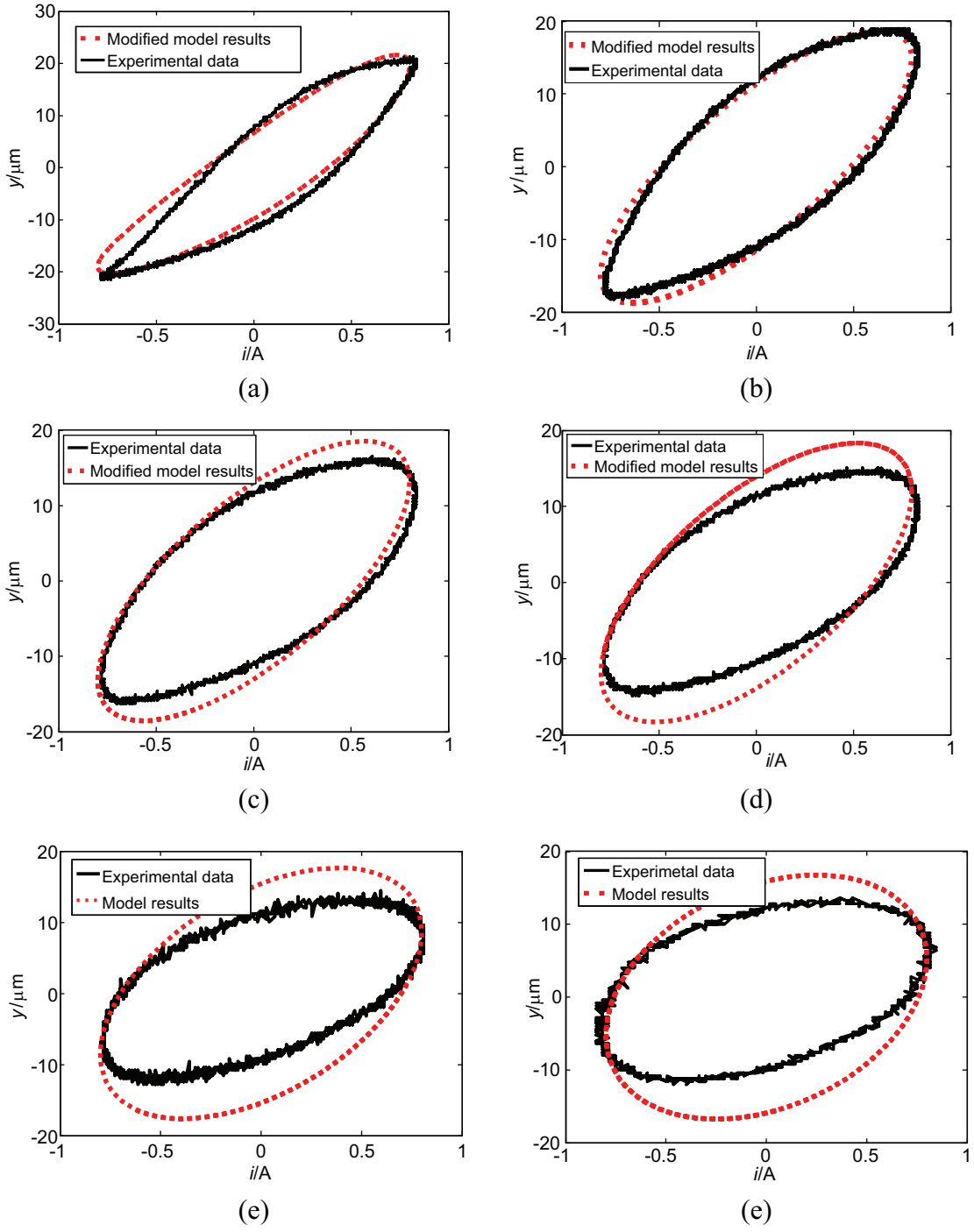

Figure 12. Verification for the dynamic modified hysteresis nonlinear model of giant magnetostrictive transducer: (a) 10 Hz, (b) 50 Hz, (c) 80 Hz, (d) 100 Hz, (e) 150 Hz, and (e) 200 Hz.

dynamic hysteresis nonlinear model considering eddy current effect, power amplifier dynamic process, and magnetic aftereffect dynamic process. After that, on the basis of experimental data, a modified quasi-static and dynamic hysteresis nonlinear model is proposed, and subsequently, the validity and reliability of the proposed modified nonlinear model are verified by quantitatively comparing its predicted results with the existing experimental data. The excellent agreements between the predicted results and experimental data indicate that nonlinear dynamic model established in this article can accurately describe the complex hysteresis behavior of the giant magnetostrictive transducer system not only under quasi-static operating conditions but also under

dynamic operating conditions of less than 100 Hz. Furthermore, the present modified hysteresis nonlinear model of giant magnetostrictive transducer in this article has the following characteristics: agree well with experimental data, computationally simple and efficient, and reasonably easy to determine transducer parameters. The present model's parameters have definite physical meaning just like the Jiles–Atherton model, but the parameters to be identified are less than those of the other hysteresis nonlinear models such as the Jiles–Atherton model. The present model's expression is more simple than that of the other hysteresis nonlinear models such as Preisach model, which is more suitable for the real-time control system, the simulation, and performance prediction of giant magnetostrictive transducer. Therefore, the research in this article provides a basic theoretical model for accurate characterization of the giant magnetostrictive transducers, which can be used in model-based active vibration control design as well.

Declaration of Conflicting Interests

The author(s) declared no potential conflicts of interest with respect to the research, authorship, and/or publication of this article.

Funding

The author(s) disclosed receipt of the following financial support for the research, authorship, and/or publication of this article: This work was supported by the National Natural Science Foundation of China (grant number 51175243), the Natural Science Foundation of Jiangsu Province (BK20131359), the Aeronautical Science Foundation of China (grant number 20130652011), and Fundamental Research Funds for the Central Universities (NS2013046).

References

Adly AA, Mayergoyz ID and Bergqvist A (1991) Preisach modeling of magnetostrictive hysteresis. *Journal of Applied Physics* 69(8): 5777–5779.

Al Janaideh M (2009) *Generalized Prandtl–Ishlinskii hysteresis model and its analytical inverse for compensation of hysteresis in smart actuators*. PhD Dissertation, Concordia University, Montreal, QC, Canada.

Aljanaideh O, Rakheja S and Su C-Y (2014) Experimental characterization and modeling of rate-dependent asymmetric hysteresis of magnetostrictive actuators. *Smart Materials and Structures* 23: 035002.

Almeida LAL, Deep GS, Lima AMN, et al. (2001) Modeling a magnetostrictive transducer using genetic algorithm. *Journal of Magnetism and Magnetic Materials* 266–230: 1262–1264.

Bertotti G (1992) Dynamic generalization of the scalar Preisach model of hysteresis. *IEEE Transactions on Magnetics* 28(5): 2599–2601.

Braghin F, Cinquemani S and Resta F (2011) A model of magnetostrictive actuators for active vibration control. *Sensors and Actuators A: physical* 165: 342–350.

Braghin F, Cinquemani S and Resta F (2012) A low frequency magnetostrictive inertial actuator for vibration control. *Sensors and Actuators A: Physical* 180: 67–74.

Calkins FT, Smith RC and Flatau AB (2000) Energy-based hysteresis model for magnetostrictive transducers. *IEEE Transactions on Magnetics* 36(2): 429–439.

Cao SY, Wang BW, Yan R, et al. (2004) Optimization of hysteresis parameters for the Jiles–Atherton model using a genetic algorithm. *IEEE Transactions on Applied Superconductivity* 14(2): 1157–1160.

Chakrabarti S and Dapino MJ (2012) Fully coupled discrete energy-averaged model for Terfenol-D. *Journal of Applied Physics* 111: 054505-1–054505-9.

Cruz-Hernandez JM and Hayward V (2001) Phase control approach to hysteresis reduction. *IEEE Transactions on Control Systems Technology* 9(1): 17–26.

Dapino MJ, Smith RC and Flatau AB (2000a) Structural magnetic strain model for magnetostrictive transducers. *IEEE Transactions on Magnetics* 36: 545–556.

Dapino MJ, Smith RC, Faidley LE, et al. (2000b) A coupled structural-magnetic strain and stress model for magnetostrictive transducers. *Journal of Intelligent Material Systems and Structures* 11: 135–152.

Engdahl G (1999) *Handbook of Giant Magnetostrictive Materials*. San Diego, CA: Academic Press.

Evans PG and Dapino MJ (2010) Efficient magnetic hysteresis model for field and stress application in magnetostrictive Galfenol. *Journal of Applied Physics* 107: 3906–3917.

Gorbet RB, Wang DWL and Morris KA (1998) Preisach model identification of a two-wire SMA actuator. In: *Proceedings of IEEE international conference on robotics and automation*, Leuven, 16–20 May, pp. 2161–2167. New York: IEEE.

Hiller MW, Bryant MD and Umegaki J (1989) Attenuation and transformation of vibration through active control of magnetostrictive Terfenol. *Journal of Sound and Vibration* 134(3): 507–519.

Hughes D and Wen JT (1994) Preisach modeling and compensation for smart material hysteresis. In: Anderson GL and Lagoudas DC (eds) *Active Materials and Smart Structures*. Bellingham, WA: SPIE, vol. 2427, pp. 50–64.

Jenner AG, Smith RJE, Wilkinson AJ, et al. (2000) Actuation and transduction by giant magnetostrictive alloys. *Mechatronics* 10: 457–466.

Jiles DC and Atherton DL (1984) Theory of ferromagnetic hysteresis. *Journal of Applied Physics* 55: 2115–2120.

Jiles DC and Atherton DL (1986) Theory of ferromagnetic hysteresis. *Journal of Magnetism and Magnetic Materials* 61: 48–60.

Jiles DC and Thoelke JB (1994) Theoretical modelling of the effects of anisotropy and stress on the magnetization and magnetostriction of $Tb_{0.3}Dy_{0.7}Fe_2$. *Journal of Magnetism and Magnetic Materials* 134: 143–160.

Karunanidhi S and Singaperumal M (2010) Design, analysis and simulation of magnetostrictive actuator and its application to high dynamic servo valve. *Sensors and Actuators A: Physical* 157: 185–197.

Kiesewetter L (1988) Terfenol in linear motors. In: *Proceedings of second international conference on giant magnetostrictive and amorphous alloys for sensors and actuators*, Marbella, 12–14 October.

Li LY, Yan BP and Zhang C (2011a) Influence of frequency on characteristic of loss and temperature in giant magnetostrictive actuator. *Proceedings of the CSEE* 31(18): 124–129.

Li YS and Zhu YC (2012) Research on displacement-sensing model and hysteresis loop of giant magnetostrictive actuator. *Journal of Mechanical Engineering* 48: 169–174.

Li YS, Zhu YC and Wu HT (2011b) Parameter optimization of jet-pipe servovalve driven by giant magnetostrictive actuator. *Acta Aeronautica et Astronautica Sinica* 32: 1336–1344.

Mayergoyz ID (1991) *Mathematical Models of Hysteresis*. Berlin: Springer.

Park WJ, Son DR and Lee ZH (2002) Modeling of magnetostriction in grain aligned Terfenol-D and preferred orientation change of Terfenol-D dendrites. *Journal of Magnetism and Magnetic Materials* 248: 223–229.

Sablik MJ and Jiles DC (1993) Coupled magnetoelastic theory of magnetic and magnetostrictive hysteresis. *IEEE Transactions on Magnetics* 29: 2113–2123.

Smith R (1997) Modeling techniques for magnetostrictive actuators. *Proceedings of SPIE* 3401: 243–253.

Tan X and Baras JS (2004) Modeling and control of hysteresis in magnetostrictive actuators. *Automatica* 40: 1469–1480.

Wakiwaka H, Aoki K, Yoshikawa T, et al. (1997) Maximum output of a low frequency sound source using giant magnetostrictive material. *Journal of Alloys and Compounds* 258: 87–92.

Wang TZ and Zhou YH (2010) A nonlinear transient constitutive model with eddy current effects for giant magnetostrictive materials. *Journal of Applied Physics* 108: 123905.

Xu H, Pei YM, Fang, et al. (2013) An energy-based dynamic loss hysteresis model for giant magnetostrictive materials. *International Journal of Solids and Structures* 50: 672–679.

Yamamoto Y, Eda H, Mori T, et al. (1997) Three-dimensional magnetostrictive vibration sensor: development, analysis, and applications. *Journal of Alloys and Compounds* 258: 107–113.

Yang F, Wen YM, Li P, et al. (2008) Resonant magnetoelectric response of magnetostrictive/piezoelectric laminate composite in consideration of losses. *Sensors and Actuators A: Physical* 141: 129–135.

Yoo JH and Wereley NM (2004) Performance of a magnetorheological hydraulic power actuation system. *Journal of Intelligent Material Systems and Structures* 15: 847–858.

Zheng XJ, Sun L and Jin K (2009) A dynamic hysteresis constitutive relation for giant magnetostrictive materials. *Mechanics of Advanced Materials and Structures* 16: 516–521.